Title: A Field Analysis of New Overhead Line Conductor Coatings to Increase Ampacity/Reduce Power Losses in Desert Environment: Performance and Durability Assessments

Authors

Dr Oliver Higbee	Dr Niall Coogan	Ahmad Al-Thagafi
AssetCool	AssetCool	GCCIA
United Kingdom	United Kingdom	Kingdom of Saudi Arabia

Key Words: Conductors, Coatings, Ampacity, Power Losses, Solar Reflectivity, Emissivity

Abstract

The peak temperature of overhead power lines limits the capacity of electricity grids: the cooler the conductor, the higher the capacity. High conductor temperatures increase resistive losses and limit the current carrying capacity of conductors, as the thermal limit is reached prematurely for a given cross sectional area. An innovative solution has emerged to reduce the temperature of overhead conductors and address these issues.

Conductor coatings cool overhead line conductors by simultaneously reflecting solar radiation and increasing heat dissipation. By reducing the amount of solar radiation a conductor absorbs whilst also substantially increasing heat dissipation, conductors can operate with a greatly reduced operating temperature for a specified current. This technology has the potential to substantially reduce transmission losses or increase current carrying capacity; especially in the regions with consistently high ambient temperatures and high levels of solar radiation that overhead conductors experience, such as GCC countries.

There are two primary parameters to explore with such a technology: performance and durability. With respect to performance, this paper reports a field trial of a bare uncoated ACSR conductor tested against a conductor coated with a proprietary conductor coating developed and patented by AssetCool. The field analysis was conducted in collaboration with the Gulf Cooperation Council Interconnection Authority (GCCIA), at the GCCIA test station in Al Fadhili, KSA. The control and test conductors were connected in series and t-type thermocouple sensors were installed. Conductor temperatures were logged alongside weather conditions through a dedicated weather station. In addition to the field investigation, the material was also tested for durability and performance in an accredited laboratory to ensure consistency of findings.

This paper concludes on the efficacy, in terms of performance, and practicality, in terms of durability, of conductor coatings as a means to reduce conductor temperatures in the GCC region.

Corresponding Author: Dr Niall Coogan, niall.coogan@assetcool.com Nexus, Discovery Way, Leeds, LS2 3AA, United Kingdom

Executive Summary

Problem this Paper Explores: Improving the Thermal Rating of Overhead Conductors

The GCC region is an environment with consistently high ambient temperatures and high levels of solar radiation. These environmental conditions limit the current carrying capacity of overhead transmission and distribution (T+D) conductors. The ampacity of overhead conductors is determined by the Maximum Allowable Conductor Temperature (MACT), beyond which excessive sag and thermal aging exceed regulatory and safety clearances.

Increasing population, economic growth, and electrification are compounding to increase the demands for improved capacity and efficiency on T+D networks. A significant component limiting improvements in capacity and efficiency is the performance of overhead conductors. Conductors with limited current carrying capacity increase the need for additional T+D infrastructure, increasing expense in power transfer.

Uncoated overhead conductors are sub-optimally efficient due to two surface phenomena: the amount of solar radiation they absorb (Solar Absorptivity, α) and the thermal emissivity (Thermal Emissivity, ε). By simultaneously absorbing significant solar radiation, whilst inefficiently radiating heat energy as infrared (IR) energy, the MACT is prematurely reached.

Solution: Spectrally Selective Coatings as a Means to improve Conductor Performance

Spectrally Selective Coatings (SSC) are coatings which minimise solar absorption and maximise thermal emissivity. 'Spectrally selectivity' refers to the coating's optimised performance in two distinct areas of the electromagnetic spectrum. These coatings operate differently to spectrally homogenous coatings such as black paints which improve thermal emissivity, but increase solar absorption, or polished surfaces which increase solar reflectivity but minimize thermal emissivity.

Research

A SSC was formulated specifically for application to overhead T+D conductors. To explore the performance and durability of the SSC in a GCC environment, a field trial rig was constructed at the Gulf Cooperation Council Interconnection Authority (GCCIA) test station, Al Fadhili, KSA. Conductors coated with the SSC were tested alongside conventional uncoated conductors.

This paper outlines the theory behind SSCs and theoretical modelling (CIGRE 601) around performance gains from optimising solar reflectivity and thermal emissivity. After this, the experimental method of the field trial and laboratory accelerated aging are described. Finally, we present the first 6 months of SSC thermal results and make comparisons of empirical vs theoretical cooling.

Results

- Peak cooling of up to 33.6% was demonstrated with average monthly temperature differences of ~6% have been demonstrated to date.
- The substantial difference between the peak cooling and the average cooling is due to the consistently high wind speeds (average 3 – 5.7 m/s on a monthly basis) at the Al Fadhili site, intentionally chosen for its harsh durability challenges (sand erosion).
- The empirical cooling demonstrated by the SSC outperforms the theoretical forecasts by CIGRE 601 by 1.1 – 2.0x, 1.38x on average.
- Accelerated testing results provide early indications of stability to a broad range of degradation phenomena.

Introduction

Macroeconomic forces are driving the need for increased transmission and distribution (T+D) capacity. Total electrical energy consumption in the GCC countries is forecasted to increase by 75% between 2020 – 2030, from 800 TWh in 2020 to approximately 1400 TWh in 2030 [1]. There is an inherent need for improving the efficiency of electricity transmission and distribution to meet this growing demand cost effectively.

A T+D system can be optimised in terms of performance and efficiency by improving the thermal rating of its overhead conductors. A key component of conductor performance is conductor temperature. Higher conductor temperatures result in a lower current carrying capacity and increased transmission and distribution losses. The Maximum Allowable Conductor Temperature (MACT) determines the maximum current carrying capacity of a specified conductor. Exceeding the MACT results in accelerated conductor aging and ultimately conductor failure due to high thermal stress [2].

Established technical brochures such as CIGRE 601 [3] highlight the effect environmental conditions have on determining the current levels at which the MACT will be exceeded (conductor ampacity). The environmental conditions in the GCC region are particularly limiting of conductor ampacity. High levels of solar radiation coupled with persistently high ambient temperatures result in higher conductor temperatures, reduced current carrying capacity and increased transmission losses. Figure 1 shows how conductor ampacity varies with ambient temperature. An increase in ambient temperature from 25 °C to 50 °C results in a 32% reduction in current carrying capacity.

CIGRE 601 is fundamentally based on steady state heat balance equations [4]. As ACSRs have a maximum continuous operating temperature of 80 °C, ambient temperatures of 50 °C leave a head room of only a 30 °C rise above the ambient temperature for the resistive heating generated by current transmission, inherently limiting the current carrying capacity of conductors.

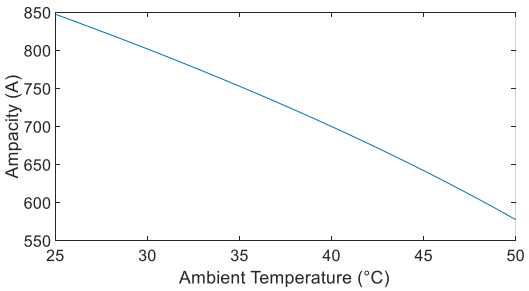

Figure 1: Conductor ampacity as a function of ambient temperature as calculated by CIGRE-601 [3]*. Conductor specification: Drake ACSR. Environmental conditions include 0.5 m/s wind speed, wind direction 45° to the conductor axis, 1000 W/m^2 Solar Radiation.*

Solutions to reduce conductor temperature are required to increase the current carrying capacity of overhead conductors.

For a conductor to cool and improve its thermal rating, these models focus on the four primary heat transfer mechanisms: convection (cooling by the wind), radiative cooling (heat dissipation by emitting thermal energy at infrared wavelengths), solar gain (heating by absorbing the sun's energy) and Joule heating (heating of the conductor by the current flowing through it) [3], [5]. This paper explores the solar and radiative components. Specifically, the extent to which minimising the amount of solar radiation absorbed (solar absorptivity, α) by a conductor, whilst simultaneously maximising the rate at which heat energy is converted into radiant energy and emitted away from the conductor's surface (i.e. maximising thermal emissivity, ε). This is achieved via the application of a spectrally selective coating (SSC) to ACSR conductors which reflects solar radiation whilst increasing surface emissivity. The key research questions are: To what extent can conductor performance be improved by optimising these surface characteristics on the conductor via a SSC? How durable is the material given the challenging environments and long lifespans of overhead transmission assets?

These questions are answered through a multi-strand research project combining the initial 6 months of results from an on-going 12-month field analysis of coated conductors in the Kingdom of Saudi Arabia, as well as laboratory testing for physical and mechanical durability via accelerated aging. As high resolution weather and conductor

temperature data are collected, we are able to make comparisons between simulated conductor temperatures and empirical conductor temperatures using the methodology presented by [6]. As well as contributing further insights on the accuracy of CIGRE 601, we can then demonstrate whether the cooling demonstrated by the coated conductor exceeds the theoretical estimates as made by CIGRE 601.

The remainder of this paper is organised as follows: firstly, brief background theory on the photonic science is provided, alongside theoretical simulations using CIGRE 601. Following this, we outline the methodology used for experimentation which is comprised of the field trial experimental design and durability testing procedure. After this, we present the results of the field trials and physical testing, before contextualising these results in relation to potential value delivered in the GCC in the discussion section. Finally, we conclude with our future research plans.

Theory

Photonics and Spectral Selectivity

Solar and infrared (IR) radiation have the potential to impact conductor ampacity. These two regions of the electromagnetic spectrum occur at different wavelengths, as demonstrated in Figure 2.

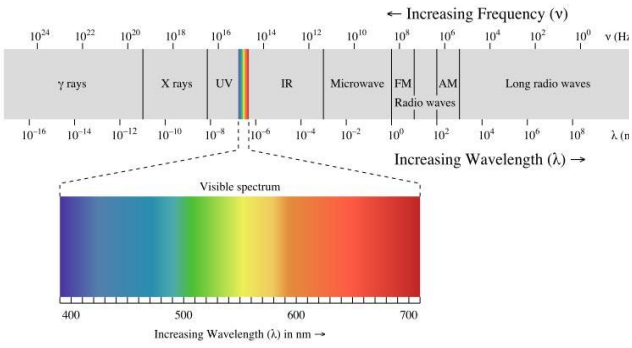

Figure 2: The electromagnetic spectrum describes light of different wavelengths, ranging from gamma rays, which are smaller than the size of an atomic nucleus, to long radio waves measuring thousands of kilometres across.

The solar radiation spectrum exists between the 0.4µm and 2.5µm comprising of UV, visible light and near infrared light. Figure 3 demonstrates the solar spectrum.

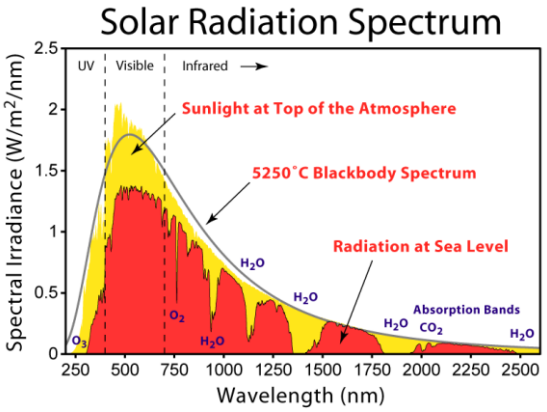

Figure 3: The Solar Radiation Spectrum is the radiation emitted from the sun, which is the spectrum emitted by a blackbody operating at a temperature of 5250°C. A small amount of this spectrum is absorbed as it enters the atmosphere, resulting in the spectrum seen in red, this is the radiation that a conductor absorbs.

At the boundary between two media (e.g. the atmosphere and a conductor surface in Figure 4) electromagnetic radiation can undergo:

a) Absorption, α: The incident radiation is transformed into another type of energy within the substrate (usually heat).
b) Reflected, ρ: The electromagnetic radiation is returned at the boundary between the two media.
c) Transmitted, τ: Electromagnetic radiation passes through the medium completely.

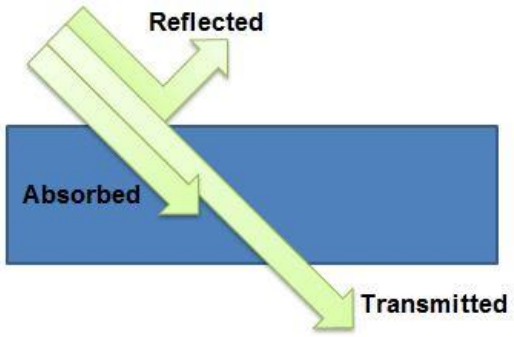

Figure 4: Interaction of light with a substrate.

The greater the absorption of solar radiation, the higher the conductor temperature. In the heat balance equation [4] which is the basis for CIGRE-601, the heat contribution from solar radiation is highlighted in Equation 1:

$$P_S = \alpha_S . D . I_S \qquad \textbf{(1)}$$

Where:

- P_S = Solar heat gain (W/m)
- α_S = Absorptivity of the surface of the conductor
- D = Conductor diameter
- I_S = Intensity of solar radiation

Conductor diameters are generally determined by design specifications based on current carrying requirements. The intensity of solar radiation is dependent on geographic location and the albedo of the ground below. The absorptivity of the surface of the conductor is not constant over the lifetime of the conductor. Generally on new lines the absorption can be 0.2/0.3 which can progress to 0.9 (e.g. 90% of solar radiation absorbed) as they darken with age [7]. Reference [7] calculates the current values accordance with EN 50341 for a standard ACSR conductor (680/73) as solar radiation increases from 100 W/m^2 to 1000 W/m^2. They demonstrate that the conductor ampacity decreases by 15.55% as the solar radiation intensity increases (EN 50341 ambient = 35°C, wind = 0.5 m/s, angle of attack = 45°).

Similar results can be demonstrated for the GCC environment, as evidence in Figure 5, where there is a 17.20% drop in conductor ampacity from 0 – 1000 W/m^2 for a Moose ACSR conductor.

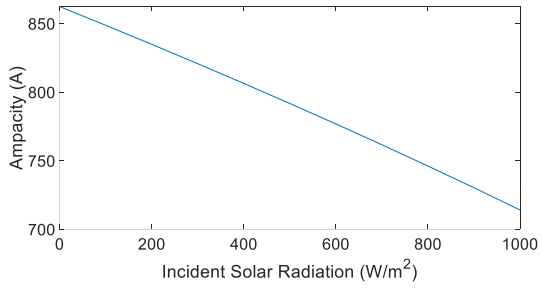

Figure 5: Moose ACSR Conductor ampacity as a function of incident solar radiation in GCC environment. Environmental conditions: 50°C, wind speed 0.61 m/s, wind direction 45° to the conductor axis, α = 0.5, ε = 0.5. Ratings guidance taken from Saudi Distribution Planning Standard [8] *calculated using CIGRE 601* [3].

The other important surface characteristic is emissivity, ε. This refers the ratio of the energy that is radiated from a material's surface to that radiated by a perfect emitter/blackbody radiator. The variable is dimensionless and varies from 0 (perfect reflector) to 1 (perfect emitter). Higher emissivity values result in a greater conversion of substrate heat energy into radiant energy followed by subsequent emission into the atmosphere, in turn cooling the substrate by emitting the heat away from the surface. The total radiative energy transmitted from the conductor's surface is given by;

$$P_r = \pi D \varepsilon_S \sigma_B [(T_S + 273)^4 - (T_A + 273)^4] \qquad \textbf{(2)}$$

Where;

- P_r = Radiation (heat) loss (W/m)
- D = Conductor diameter
- ε_S = Emissivity coefficient of conductor surface
- σ_B = Stefan-Boltzmann constant
- T_S = Conductor temperature
- T_A = Ambient temperature

Seminal references [9], [10] explored the implications of conductor emissivity increasing over time as the conductor weathers. This has led to many utilities adopting emissivity values of 0.8/0.9 for weathered conductors. However, recent research has demonstrated 32 year old conductors with emissivity values of 0.45 [11], [12] calling into question the validity of these assumptions, and highlighting the variable nature of surface weathering on increasing surface emissivity over time.

First Principles Photonic Optimisation - Spectral Selectivity

The theory above outlines the potential benefits from a) minimising solar radiation, b) maximising thermal emissivity and c) fixing these values over time to allow for confidence when deciding the thermal rating of overhead lines. With conventional materials however, emissivity is taken to be the inverse of reflectivity on substrates where transmittance is negligible, i.e. increasing emissivity increases absorptivity. Spectrally selective materials address this problem via the optimisation of these two properties simultaneously.

This is critical, as some materials are highly emissive (*e.g.* a black paint) but absorb strongly in

the solar region, which drives conductor temperatures up and mitigates radiative cooling effects. Other materials, such as shiny/polished metals, are highly solar reflective but poorly emissive, resulting in ineffective heat dissipation, leading to an increase in substrate temperature due to an inability to radiate the heat energy generated by Joule heating. Hence, the material specified must have both high solar reflectance and high thermal emissivity. This is demonstrated in Figure 6.

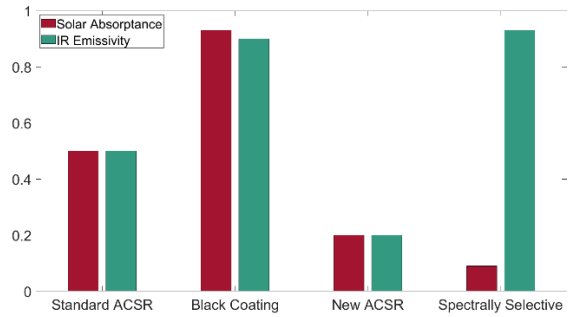

Figure 6: The solar absorptance (red) and IR emittance (green) of different surfaces. A new conductor reflects the sun's energy but is ineffective at dissipating heat. The black paint is a strong emitter, ideal for cooling at night but will heat up in the day as it strongly absorbs the sun's radiation. Standard ACSR are the Absorptance and Emissivity used in thermal rating standards. The spectrally selective coating reflects the sun's energy and strongly emits; the optimal surface property for a conductor in low wind conditions.

Another way to view spectral selectivity is demonstrated in Figure 7. This ideal spectral profile explains that a material should have minimal absorption (maximum reflection) in the solar spectrum (0.4µm – 2.5µm) and at wavelengths greater than 2.5µm have maximum absorption. Absorption is equal to emissivity in this steady state case. This way, the material will passively optimise the incoming and outgoing radiation to cool the conductor and increase thermal ratings.

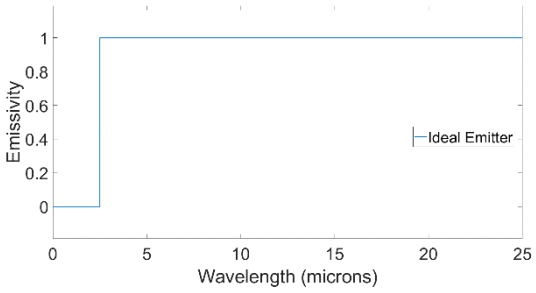

Figure 7: Ideal emitter for maximising conductor cooling.

Theoretical Simulations According to CIGRE 601

The parameters of solar absorptivity and thermal emissivity are standard input variables in thermal rating calculations. Thus, it is feasible to simulate the effects of reducing solar absorption and increasing thermal emissivity. In this section, we use existing thermal rating calculators [3] to theoretically predict performance in the GCC environment using ratings guidance from GCC member states. In addition to this single point deterministic calculation, we will use the methodology demonstrated by [6] in order to compare the theoretical predictions with actual empirical weather data to look at the accuracy of the forecasting models.

It can also be demonstrated how minimising solar absorption and maximising thermal emissivity improves conductor performance across varying environmental conditions. Figure 8 plots the change in Moose ACSR conductor ampacity with increasing solar radiation from 0 to 1000 W/m^2 with a fixed ambient temperature (50°C). The linear regression equations describing the lines in Figure 8 are expressed below. With equation (3) describing the spectrally selective coated conductor and equation (4) for the uncoated conductor.

$$y = -0.0248*x + 954 \quad \textbf{(3)}$$

$$y = -0.1482*x + 864 \quad \textbf{(4)}$$

Table 1: Environmental conditions assumed for "Summer and Winter Scenarios".

	SSC	Standard	SSC	Standard
Season	Summer		Winter	
Conductor[1]	Drake ACSR		Drake ACSR	
Emissivity	0.93	0.5	0.93	0.5
Solar Absorptivity	0.1	0.5	0.1	0.5
Ambient Temperature	50°C		25°C	
Solar Radiation	1000 W/m^2		600 W/m^2	
Wind Speed	0.61 m/s		0.61 m/s	
Wind Direction	45°		45°	

The gradient of the linear regression equation is -0.02 for the coated conductor and -0.15 for the uncoated conductor, thus suggesting the coated conductor loses ampacity 6 times slower than the uncoated conductor when solar radiation increases. For example, the ampacity of the uncoated conductor decreases by 30 Amps for every 200 W/m^2 increase in solar radiation, compared with just 5 Amps with an SSC applied.

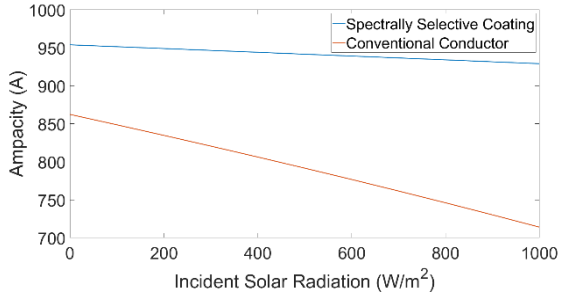

Figure 8: Moose ACSR conductor ampacity as a function of incident solar radiation in GCC environment. Environmental conditions: 50°C, wind speed 0.61 m/s, wind direction 45° to the conductor axis for a) uncoated conductor $\alpha = 0.5$, $\varepsilon = 0.5$ and b) SSC conductor $\alpha = 0.1$, $\varepsilon = 0.93$. Ratings guidance taken from Saudi Distribution Planning Standard [8] *calculated using CIGRE 601* [3].

Methodology

This section outlines the methods for the following areas: a) field analysis of performance b) laboratory analysis of coating durability and c) data analysis including comparison of theoretical vs empirical cooling performance as simulated by CIGRE 601 [3].

[1] All electrical and mechanical properties of the conductor are consistent across cases.

Field Analysis of Performance

A dedicated field trial testing span was constructed at GCCIA Test Station in Al Fadhili, Kingdom of Saudi Arabia. Six 7.5m Quail ACSR/AS conductors were sourced. Three were coated with a proprietary SSC formulated specifically for overhead conductors. The SSC-conductors were treated as the test conductor. The remaining three conductors were left as received and treated as the control conductor. Three of each conductor sample were used to analyse the consistency of samples. The six conductors were suspended from 7m distribution poles and connected electrically in series. The circuit was then connected to 4x1500w direct current, remotely programmable (DC) power supplies (Kikusui PWX1500L) able to supply up to 600A DC or up to 30V DC. The aim of the trial was to determine thermal performance in desert environments and as such low voltage was chosen to keep current high and allow for flexibility of installation sites.

T-type thermocouples were inserted into the conductor cores (8 per line), and these were connected into a National Instruments CompactDAQ Chassis (cDAQ-9178) *via* conditioned modules (3xNI-9213 Spring Terminal TC modules). Further, a dedicated weather station (ClimaVUE50) was installed on site to capture high resolution weather data, including air temperature, wind speed, wind direction and solar radiation, the necessary inputs for the CIGRE 601 model [3]. This design (use of high current, low volts DC with T-type thermocouples inserted into the conductor core for temperature measurement) is a consistent experimental set up to a multi-year conductor temperature study in the UK conducted by a Distribution Network Operator aimed at improving the statistical ratings guidance for overhead lines and thus we conclude it is in line with good industry practice [13].

This experimental design ensures the test and control conductors experience the same current, as they are connected electrically in series. Furthermore, the lines are equally spaced (0.75m) and of the same orientation to the wind and the sun, hence we can assume environmental variables

are constant across all conductors. Therefore, we can deduce that any conductor temperature differences are due to the different surface properties, e.g. the presence of a SSC. As of submission, the 12-month field trial is ongoing. Initial results from April 2021 – September 2021 are illustrated and analysed below. The remaining data will be analysed in a future publication as outlined in the future research section.

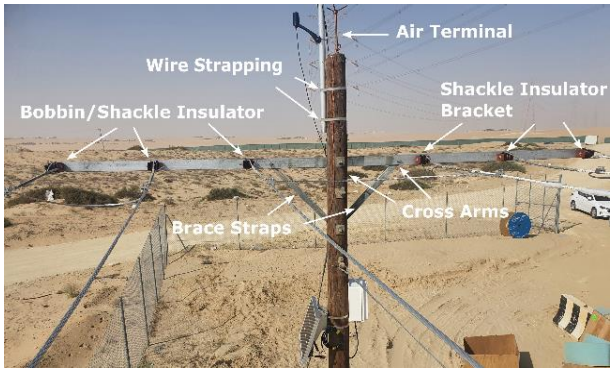

Figure 9: Field trial cross arm set up.

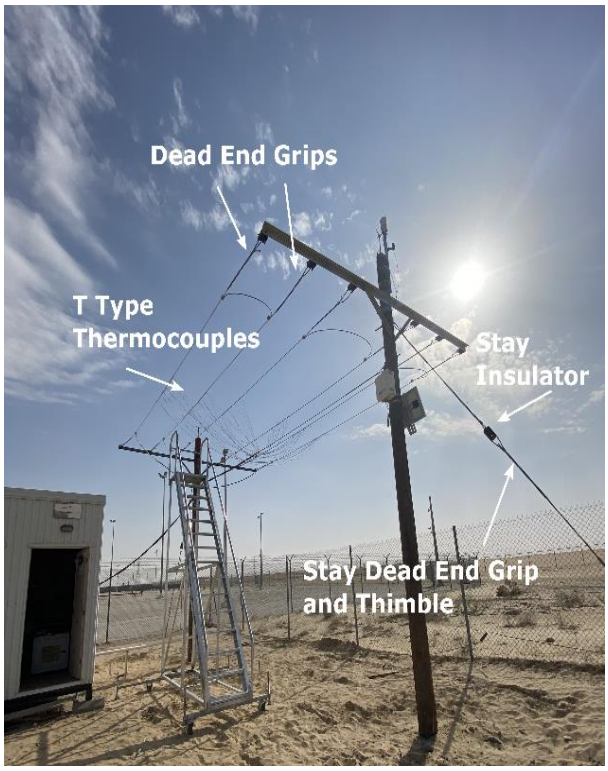

Figure 10: Field trial testing span constructed at GCCIA Test Station in Al Fadhili, Kingdom of Saudi Arabia.

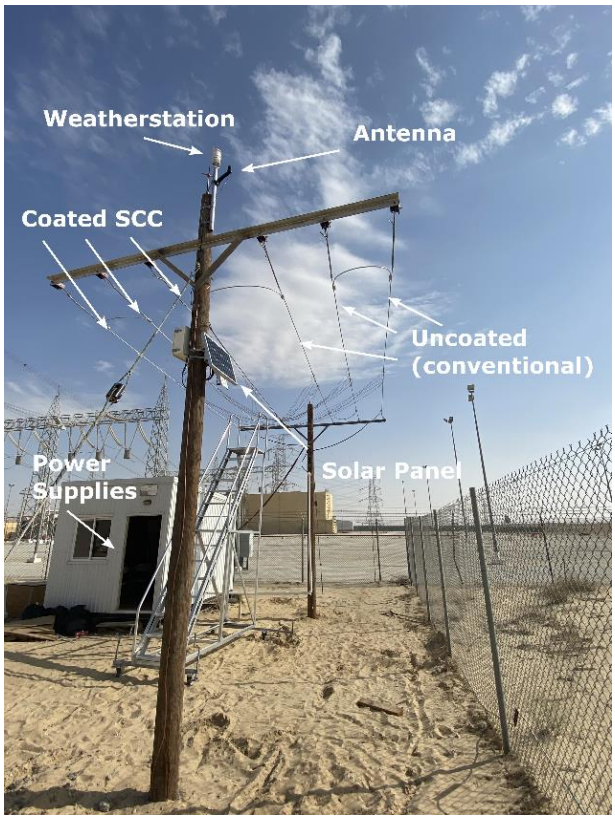

Figure 11: Field trial testing span constructed at GCCIA Test Station in Al Fadhili, Kingdom of Saudi Arabia.

Laboratory Testing of Durability: Accelerated Aging

Transmission assets have long asset life cycles (upwards of 30 years). It is important to demonstrate any tested material has the appropriate durability and stability under a wide variety of environmental stresses. These are now discussed in turn. It should be noted many of these durability tests are ongoing at the time of publication and extended accelerated aging will be discussed in "Future Work" section.

UV Stability: Operating in the GCC environment over many decades requires that a material has a strong resistance to UV radiation. This was tested by ASTM G155 UV accelerated aging for 1000 hours. After the exposure, Grey Scale evaluations according to ISO 105-A02:1993 were performed.

Corrosion Stability: The atmosphere in many regions can be highly corrosive, especially in desert and coastal atmospheres. The coating was tested to ASTM B117 for 500 hours. After the exposure, Grey Scale evaluations according to ISO 105-A02:1993 were performed.

Temperature Stability: The SSC was applied to an aluminium Q-panel. After curing, the sample was placed in an oven at 150°C for 3 days. The sample was examined for any cracking, flaking or discolouration etc. after the testing period.

Chemical Stability: Power lines operate a high temperature and are subject to high moisture environments either via humidity or rain. In regions where there are high levels of pollutants in the atmosphere, particularly sulphur dioxide, this rain can have a lower pH and become acidic. It is important to demonstrate that the coatings are stable to moisture with a pH comparable to acid rain without degrading. Normal rain typically has a pH of 5 – 5.5. Acid rain typically has a pH of around 4. This was tested according to EN 598+A1-2009. Coated samples were subjected to immersion in aqueous sulfuric acid (pH 3) and sodium hydroxide (pH 13), which was circulated at a flow rate of 1 L/min at a constant temperature of 18 °C for 7 days. Subsequent visual inspection of the coating was then carried out to determine any detrimental effect.

Moisture Stability: Moisture stability was tested via the ASTM D870 water submersion test for 48h at 38°C.

Humidity Stability: In tropical regions, sustained levels of high humidity (over 80%) are feasible. This can accelerate corrosion, especially in coastal areas. To test the stability in such environments, the coating was inserted into a 100% RH atmosphere for 2 days according to ASTM D2247. The coating achieved a pass in this test if there was no film discoloration, cracking, flaking or chipping after the test.

Sulphur Dioxide Resistance: Due to the risk of acid rain in industrial environments, resistance to moist SO_2 was tested via ASTM G87, two cycles, method B.

Comparisons with CIGRE 601

The final analysis section in this paper explores the temperature calculation of overhead powerline ACSR conductors according to the methodology stated in CIGRE technical brochure 601: Guide for thermal rating calculations of overhead lines [3]. The field trial involved the collection of high-resolution weather data and high-resolution conductor temperature data. This permits the calculation of a theoretical conductor temperature using the empirically recorded weather variables. The calculated temperature is compared to the empirical temperature data collected in this project.

This represents an opportunity to a) compare the cooling performance in relation to theoretical expectations and b) add to the body of literature comparing the efficacy of thermal ratings calculators as effective models for determining conductor temperature [5], [6] in GCC conditions.

The objective of CIGRE Technical Brochure 601 is to calculate the thermal rating of overhead lines. It takes weather conditions and conductor properties and utilises them to model conductor temperature and predict ampacity. 601 builds on CIGRE TB 207 to include lines that operate at high current densities and temperatures.

Here we investigate coated conductors on DC lines. For a steady state, the thermal rating of a line is determined by a point of thermal equilibrium, whereby a temperature is reached when cooling and heating mechanics balance each other out. For a DC conductor these mechanics can be expressed by;

$$P_J + P_S = P_C + P_R \qquad \textbf{(5)}$$

Where the left side are sources of heating; P_J is Joule heating (the heating of the conductor by the current flowing through it) and P_S is solar heating (heating of the conductor by absorbing the sun's energy). The right side of the equation are sources of cooling: P_C is convective cooling (transporting heat away from the conductor by the air moving over it) and P_R is radiative cooling (cooling of the conductor by emitting heat away).

Joule heating is given by;

$$P_J = I^2 R_{dc20}(1 + \alpha_{TR}(T_S - 20)) \qquad \textbf{(6)}$$

Where;

- I = Conductor current
- R_{dc20} = Conductor DC resistance at 20°C
- α_{TR} = Temperature coefficient of resistance
- T_S = Conductor Temperature

The temperature coefficient of resistance was approximated to that of aluminium given that including the steel core altered this value by 0.01% [14].

Solar heating is given by equation (1), Radiative cooling by equation (2) and convective cooling by equation (7);

$$P_c = \pi\lambda_f(T_S - T_A)\,Nu \qquad \textbf{(7)}$$

Where;

- P_c = Convection (heat) loss (W/m)
- λ_f = Thermal conductivity of air
- T_S = Conductor temperature
- T_A = Ambient temperature
- Nu = Nusselt number

Equation (5) and (6) can be rearranged to give a thermal rating by setting T_s to MACT (maximum allowable conductor temperature).

$$I_{max} = \sqrt{\frac{P_C + P_R - P_S}{R_{dc20}(1 + \alpha_{TR}(T_S - 20))}} \qquad \textbf{(8)}$$

Or T_s can be calculated by rearranging (8). Note that P_c and P_r have T_s dependence, therefore calculating T_s requires additional iterative/optimisation steps.

A global approach to optimisation was taken by iterating each weather parameter over the tolerance range of the weather station and simultaneously iterating over the tolerance of the thermocouples and power supply. The resolutions and accuracies are given in the Table 2.

Table 2: Resolution/accuracies for CIGRE 601 Optimisation.

Parameter	Resolution	Accuracy
Air Temperature	0.1°C	±0.6°C
Wind Speed	0.01 m/s	±3% or ±0.3 m/s
Solar Radiation	1 W/m²	±5%
Wind Direction	1°	±5°
Conductor temperature	0.1°C	±1°C
Measured Current	0.5A	±0.5%

Tolerances for wind direction were increased to include installation of the weather station error of ±20°. The optimisation model was then compared with empirical values and the closest fit was chosen.

Data Analysis

Descriptive Weather Statistics

Table 3 includes the monthly descriptive weather statistics since the weather station has been installed at site. Al Fadhili test station was chosen specifically due to the harsh conditions, primarily high wind speeds, which regularly induce sand-based erosion. Accordingly, monthly average wind speeds of 3.0 m/s – 5.7 m/s have been recorded.

Tables 4 and 5 separate these recordings by day and night. It is visible that consistently high wind speeds are recorded during the day (3.9 m/s – 7.2 m/s) on average. Table 6 shows the large range in weather conditions seen at Al Fadhili, with temperatures starting at 5.4°C and peaking at 49.7°C. High wind speeds up to 19.9 m/s have been recorded and the relative humidity has varied between 5% and 100% (rain). Solar radiation up to 950 W/m² was also seen. These ranges underline the harsh conditions the conductors have encountered.

Table 3: Monthly Averages.

	Amb* (°C)	Wind Speed (m/s)	SR (W/m²)	RH (%)
Apr	28.0	4.0	207.7	30.9
May	34.0	3.2	234.5	22.4
Jun	36.4	5.7	203.7	20.2
Jul	38.0	3.3	220.9	31.3
Aug	37.1	3.0	198.9	34.2
Sep	33.8	3.8	175	38.1

**Amb – ambient temperature, SR – solar radiation, RH – relative humidity.*

Table 4: Monthly Daylight Weather.

	Amb* (°C)	Wind Speed (m/s)	SR (W/m²)	RH (%)
Apr	30.7	5.0	376.9	24.9
May	36.9	4.1	404.4	17.5
Jun	38.9	7.2	349.6	17.1
Jul	40.6	4.3	381.1	25.4
Aug	40.0	3.9	359.6	26.8
Sep	36.9	5.2	332.9	29.4

Table 5: Monthly Night-time Weather.

	Amb* (°C)	Wind Speed (m/s)	SR (W/m^2)	RH (%)
Apr	24.6	2.9	0.0	38.3
May	30.1	2.0	0.0	29.2
Jun	33.1	3.6	0.0	24.6
Jul	34.4	1.9	0.0	39.5
Aug	33.5	1.9	0.0	43.4
Sept	30.4	2.3	0.0	47.7

Table 6: Minimum and Maximum Weather readings recorded (averaged over one minute).

	Amb* (°C)		WS*	SR*	RH (%)	
	Min	Max	Max	Max	Min	Max
Apr	14.3	42.6	18.8	925	6.5	96.8
May	21.4	48.5	12.5	950	5.3	76.8
Jun	26.3	49.1	19.9	800	6.2	62.6
Jul	26.0	49.5	11.8	874	6.8	100
Aug	26.5	49.7	11.7	729	7.8	85.5
Sept	23.5	47.4	14.0	668	8.7	94.3

**WS – Wind speed (m/s), SR – solar radiation* (W/m^2), *RH – relative humidity.*

High wind speeds have a large effect on the cooling as seen in this region. To illustrate this, equation (1) is used to calculate heating power from solar radiation and equation (7) to calculate cooling power from the wind.

By plotting solar heat gain against convection heat loss, it can be seen in Figure 12 that convection loss is a lot more dominant. It is expected that the conductors will be hotter when wind speeds are low regardless of what the solar intensity is. Looking at Table 4 and 5, wind speeds are significantly lower at night, so conductor temperatures are expected to be higher during this time. It can be predicted that the coating will have a larger impact on the temperature of the conductor at night because radiative cooling power becomes more dominant as convective cooling power drops.

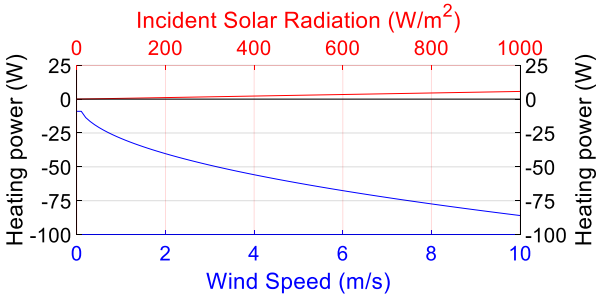

Figure 12: Heating power of solar gain compared to cooling power of convection.

At higher wind speeds, convective cooling dominants, resulting in a smaller average temperature difference between coated and uncoated conductors, as shown in Figure 13. Figure 13 demonstrates that moving from 0.5 m/s to 10 m/s wind speeds, the temperature difference between coated and uncoated conductors will exponentially decrease from over 20°C to 5.5°C as wind speeds reach 5 m/s. This difference further reduces to less than 3°C at 10 m/s. Whilst this lowers the average temperature difference over time, it does not limit the value of the SSC as the periods of low wind are challenging to predict spatially (along the conductor) and temporally with respect to weather forecasts. Errors in ratings with respect to low winds can cause thermal aging and catastrophic conductor failure [2].

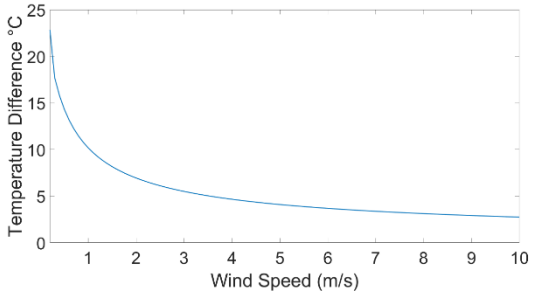

Figure 13: Temperature difference between SSC Conductor and Conventional ACSR as a function of wind speed, as calculated by CIGRE-601 [3]. Model Parameters: Quail ACSR/AS, wind direction 45° to the conductor axis, 500 W/m^2 Solar Radiation, 40°C Ambient Temperature, 380A DC current.

Accelerated Laboratory Testing

The results for the laboratory accelerated aging are included in Table 7. As we can see, in these early stages of accelerated aging the SSC looks resistant to many of the forces which may degrade the film. Significantly more data collection is ongoing and will be reported in a future publication.

Table 7: Results from laboratory accelerated aging.

Test	Result
UV-ASTM G155	5 (no change in colour according to ISO105-A02). No indentations, chipping, flaking.
Corrosion – ASTM B117	5 (no change in colour according to ISO105-A02). No indentations, chipping, flaking or discolouration.
Temperature Stability	Pass - No indentations, chipping, flaking or discolouration.
Chemical stability – EN 598	Pass - No cracking, no foaming, no peeling
Moisture Stability – ASTM D870	Pass - No cracking, no foaming, no peeling
Humidity Stability – ASTM D2247	Pass - No colour change, no blisters
SO_2 Resistance – ASTM G87	No pits, no cracks, no blisters

SSC Cooling Data

This section outlines the cooling data recorded. Both monthly averages and peak cooling data are presented. Due to the consistently high wind speeds, the lines are regularly cooled by convection. Table 8 highlights that the average cooling over the monthly periods was 2.50 – 8.27%.

Table 9 and 10 split the monthly trends into day and night periods with the average cooling being much higher at night (5.33-10.38%), due to the lower wind speeds experienced at night resulting in reduced convective cooling and increasing dominance of radiative cooling.

Table 8: Average monthly conductor temperatures and cooling.

	Conventional	SSC	Cooling (%)
April	64.92	59.55	8.27
May	65.11	60.49	7.11
June	57.57	56.13	2.50
July	67.35	64.13	4.79
Aug	67.72	64.04	5.43
Sept	61.27	57.86	5.57

Table 9: Average monthly Daytime conductor temperatures and cooling.

	Conventional	SSC	Cooling (%)
April	63.19	59.15	6.39
May	62.66	59.70	4.73
June	53.67	53.58	0.16
July	64.93	62.91	3.10
Aug	65.28	63.22	3.16
Sept	57.77	56.34	2.46

Table 10: Average monthly Night-time conductor temperatures and cooling.

	Conventional	SSC	Cooling (%)
April	66.97	60.01	10.38
May	68.37	61.53	10.04
June	63.13	59.76	5.33
July	70.59	65.75	6.86
Aug	70.76	65.08	8.03
Sept	65.06	59.49	8.55

An example cooling day is demonstrated in Figure 14. The blue line denotes the average of the 3 lengths of Quail ACSR/AS with a spectrally selective coating (SSC) applied. The grey line is the average of the 3 conventional Quail ACSR/AS spans and yellow the ambient air temperature. As seen, the SSC lines remained consistently below the conventional lines, with the largest differences seen when the temperature peaks in periods of low wind. These spikes are critical periods to cool. Here we run the spans at 380A, far above the recommended thermal rating. The conventional conductor regularly exceeded the MACT whereas the SSC remained below this crucial threshold.

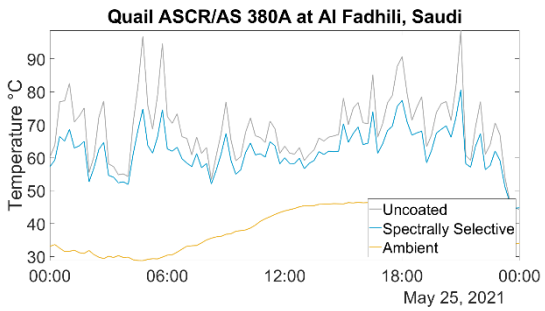

Figure 14: Coated and uncoated Quail ASCR/AS conductor temperatures in Al Fadhili, Saudi at 380A DC. Ambient Air temperature shown in gold. Average Metrological data. Wind Speed =2.7 m/s, Direction = 0° Solar Radiation =216 W/m².

By focusing on periods where convective cooling is low, the effect of the SSC can be seen. Figure 15 shows a 4 hour period during the day with wind speeds between 1.3 m/s and 2.2 m/s. Here the lower solar gain and higher radiative cooling afforded to the SSC lines are more visible.

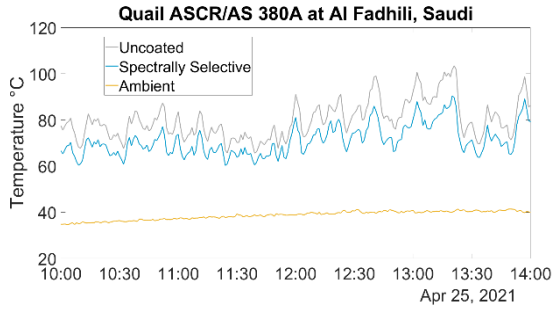

Figure 15: Coated and uncoated Quail ASCR/AS conductor temperatures in Al Fadhili, Saudi at 380A DC. Ambient Air temperature shown in gold. Average Metrological data. Wind Speed =1.75 m/s, Direction = 30° Solar Radiation =670 W/m².

Peak cooling outlines the temperature reduction in "worst case scenario conditions" to which conductors are regularly rated. *e.g.* low wind, high solar radiation and high ambient temperatures. The peak cooling periods for each month is shown in Table 11. Peak cooling temperatures of 19.1% - 33.6% have been demonstrated. It should be noted these peaks were recorded in weather conditions far from the worst-case scenario conditions outlined in the summer scenarios (1.1-2.1 m/s wind, 0 W/m solar, 23.6-33.6°C ambient), meaning larger cooling peaks are predicted during the course of this field trial.

Table 11: Peak cooling periods in each month.

Time Stamp	Bare	SCC	Cooling
28 April 04:37	103.5	78.9	23.7%
04 May 22:34	105.3	76.5	27.4%
09 June 21:26	100.1	78.9	21.2%
30 July 04:31	88.0	71.2	19.1%
31 August 07:27	100.8	67.2	33.6%
02 September 06:01	79.6	57.3	28.0%

Table 11 also illustrates a key phenomenon of the SSC. The conventional conductor has clearly exceeded the MACT and the capacity of the network would have to decrease until the conductor temperature is below MACT. However, with an SSC, the current on the test span did not have to be decreased and capacity would not be affected. It can be seen that without the SSC exceeding MACT (80°C), the cooling performance has been measured up to 33.6%. Another key advantage of the SSC is power savings, using the differences in resistance caused by the difference in operating temperatures between the conductors, power savings (I^2R) were calculated on peak cooling days and extrapolated out to a kilometre span as shown in Table 12. It can also be seen in the first two quarters of the project there has been no decrease in peak cooling performance.

Table 12: Power loss savings calculated from lower operating temperature.

Time Stamp	Bare	SCC	Cooling	Power savings per km (kWh)	% Power Loss Savings
23 April	74.0	65.9	10.9%	45.2	2.6
24 May	78.8	70.7	10.3%	45.6	2.5
01 June	64.1	60.9	5.1%	18.5	1.0
22 July	76.2	69.8	8.5%	36.3	2.1
18 August	71.9	66.5	7.6%	30.7	1.8
09 Sept	77.9	70.4	9.7%	42.5	2.5

Comparisons with CIGRE 601

Using the method outlined above, we seek to model the temperatures of the test conductors and see alignment to empirically recorded temperatures. Here we take an example day in each of the three months and perform dynamic thermal rating calculations for both the SSC and conventional conductor.

The graphs are included in Figures 16-24. The data is summarised in Table 13.

Table 13: Comparison of empirical vs modelled temperature for six sample days.

	Line type	Empirical Temperature	Modelled temperature	% Difference
23 Apr	Conventional	74.0	83.3	11.2
	SSC	65.9	76.4	13.7
24 May	Conventional	78.8	85.3	7.6
	SSC	70.7	79.7	11.3
01 June	Conventional	64.1	67.3	4.8
	SSC	60.9	65.1	6.5
22 July	Conventional	76.2	81.5	6.5
	SSC	69.8	75.4	7.4
18 August	Conventional	71.9	77.0	6.6
	SSC	66.5	72.2	7.9
09 Sept	Conventional	77.9	78.6	0.9
	SSC	70.4	74.7	5.8

Whilst the alignment between theoretical and empirical are aligned in Figures 16-24, the % alignment is generally lower than that reported by [6]. With respect to the conventional conductor theoretical predictions are 0.9 – 11.2% higher than empirical data. With respect to SSC conductors, the theoretical temperature is 5.8 – 13.7% higher than the empirical temperatures. These temperature differences could be due to the unique aspects of the GCC climate or the need to more accurately model coating cooling mechanics for conductors as opposed to simply changing solar absorptivity and thermal emissivity in the model. We seek to explore these theoretical differences in greater detail in a future paper, as outlined in our future research section.

A critical benchmark for the coating is whether the empirical cooling exceeded the theoretically predicted cooling generated in CIGRE 601. In exceeding this cooling, network operators can confidently rate SSC conductors. This analysis is demonstrated in Table 13.

Table 14: Comparison of empirical vs CIGRE 601 modelled temperature difference.

	Empirical Temperature Difference (°C)	Theoretical Temperature Difference (°C)	Out-performance of CIGRE 601 Predictions
23 April	8.0	7.0	1.14x
24 May	8.1	5.6	1.45x
01 June	3.3	2.2	1.50x
22 July	6.4	6.1	1.06x
18 August	5.5	4.8	1.14x
09 Sept	7.5	3.8	1.97x

The results demonstrate the SSC outperformed predictions from CIGRE 601 by 1.1 – 2.0x, 1.38x on average. This provides evidence at this early stage that the ampacity calculations derived in Table 15 below are conservative estimations of the ampacity increase available from SSC conductors. Using CIGRE 601 the following ampacity increases are demonstrated.

Table 15: Drake ACSR ampacity increases in summer and winter in KSA modelled by CIGRE 601.

	SSC	Standard	SSC	Standard
Season	Summer		Winter	
Conductor[2]	Drake ACSR		Drake ACSR	
Emissivity	0.93	0.5	0.93	0.5
Solar Absorptivity	0.1	0.5	0.1	0.5
Ambient Temperature	50°C		25°C	
Solar Radiation	1000 W/m^2		600 W/m^2	
Wind Speed	0.61 m/s		0.61 m/s	
Wind Direction	45°		45°	
Ampacity increase from SSC	172A 28.3%		131A 19.9%	

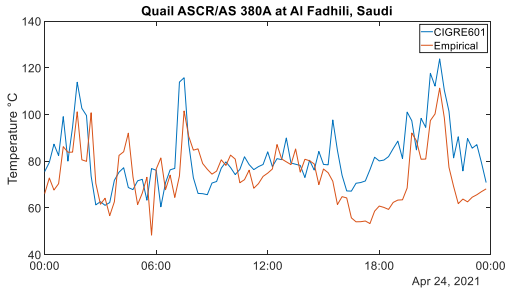

Figure 16: Empirical and modelled conventional conductor temperatures for April 24th 2021.

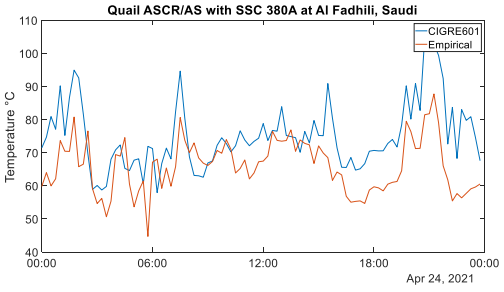

Figure 17: Empirical and modelled SSC conductor temperatures for April 24th 2021.

[2] All electrical and mechanical properties of the conductor are consistent across cases.

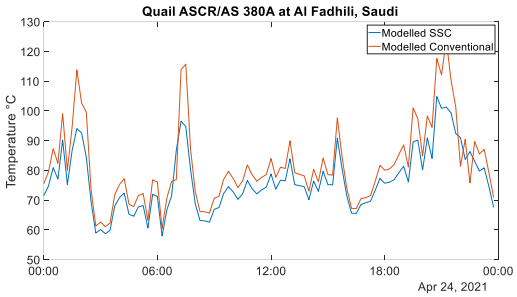

Figure 18:Modelled conventional and SSC conductor temperatures for April 24th 2021.

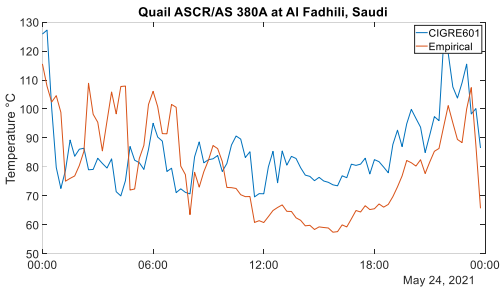

Figure 19: Empirical and modelled conventional conductor temperatures for May 24th 2021.

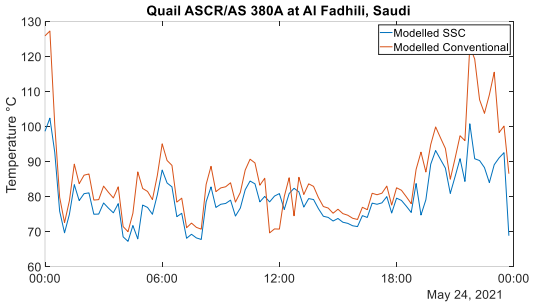

Figure 20: Modelled conventional and SSC conductor temperatures for May 24th 2021.

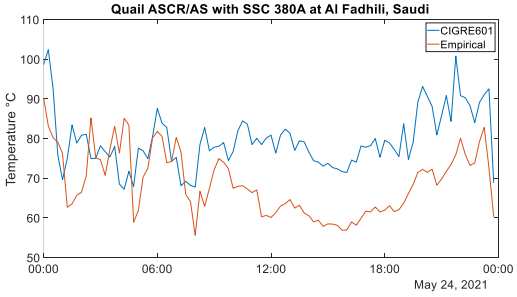

Figure 21: Empirical and modelled SSC conductor temperatures for May 24th 2021.

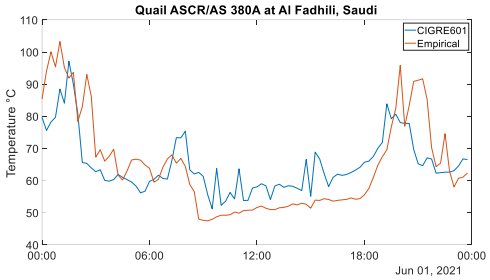

Figure 22: Empirical and modelled conventional conductor temperatures for June 1st 2021.

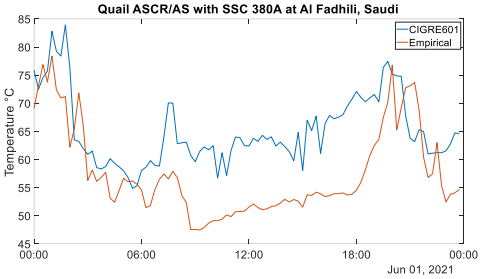

Figure 23: Empirical and modelled SSC conductor temperatures for June 1st 2021.

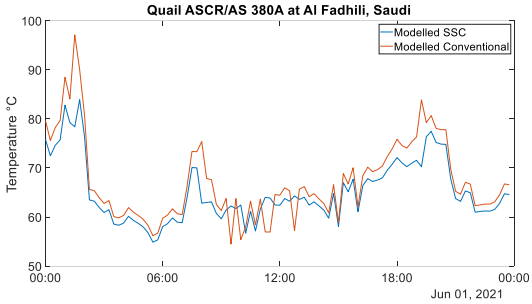

Figure 24: Modelled conventional and SSC conductor temperatures for June 1st 2021.

Future Work

This research will continue over the coming 12 months and seek to report on the following in the future:

Firstly, continuing the field trial for a full 12 months in GCC conditions will provide performance data in all seasons. In addition to this, it will allow for side by side performance comparisons of brand new SSC coated conductors compared to those that have been in the field for the field trial. Accordingly, using large scale correlation plots an indication of performance consistency will be provided.

In addition to this, accelerated laboratory aging will continue to collect as much data on UV and corrosion stability as possible. A dedicated

publication on the durability analysis of coatings in GCC and high voltage environments will be presented to add to the growing body of literature analysing the durability of coatings in these environments [15], [16].

The work reported attempting to align empirical temperatures to theoretical temperatures generated by CIGRE 601 requires further exploration as more divergence was seen than reported by [6]. Understanding the significant variables with respect to deviation at the Al Fadhili test site is another research project of interest. This may be due to GCC specific weather conditions which may require an update to the CIGRE 601 brochure on a regional basis. This is to be explored.

Conclusion

This paper reports the initial results of a field trial of a conductor with an SSC compared to an uncoated conductor. Up to 34% cooling was demonstrated with average cooling of ~6% on a monthly basis. The significant disparity between the average cooling and the peak cooling was due to the consistently high wind speeds experienced to date in the field trial, disproportionately cooling the conductors.

Despite the consistently high wind speeds, the empirical cooling demonstrated by the SSC outperformed theoretical simulations by CIGRE by up to 2.0x. This provided early evidence that standard industry calculators are a conservative estimate of SSC performance compared to an uncoated conductor and may be used to indicate potential ampacity gains of up to 30% in GCC conditions.

Early durability data has been presented and will continue in parallel with the trial. At the conclusion of the trial side by side analysis between a 12-month field aged conductor and a brand new conductor will provide performance insights on consistency of cooling in the GCC environment.

References

[1] A. Al-Badi and I. AlMubarak, "Growing energy demand in the GCC countries," *Arab J. Basic Appl. Sci.*, vol. 26, no. 1, pp. 488–496, 2019.

[2] O. Armstrong, G. Southern, A. Carroll, and G. O'Brien, "Low wind speed occurrences and aging conductors: More than just a sag problem?," in *2018 IEEE/PES Transmission and Distribution Conference and Exposition (T&D)*, 2018, pp. 1–5.

[3] T. B. Cigré, "601," *Guid. Therm. Rat. Calc. Overhead Lines, Work. Gr. B*, vol. 2, p. 43, 2014.

[4] V. T. Morgan, "The thermal rating of overhead-line conductors Part I. The steady-state thermal model," *Electr. power Syst. Res.*, vol. 5, no. 2, pp. 119–139, 1982.

[5] A. Arroyo *et al.*, "Comparison between IEEE and CIGRE thermal behaviour standards and measured temperature on a 132-kV overhead power line," *Energies*, vol. 8, no. 12, pp. 13660–13671, 2015.

[6] M. Kanálik, A. Margitová, and Ľ. Beňa, "Temperature calculation of overhead power line conductors based on CIGRE Technical Brochure 601 in Slovakia," *Electr. Eng.*, vol. 101, no. 3, pp. 921–933, 2019.

[7] M. ŠPES and M. MÁRTON, "The impact of solar radiation for maximum current load of 400 kV power lines."

[8] SEC, "Saudi Distribution Planning Standard, DPS-03," 2015.

[9] W. S. Rigdon, H. E. House, R. J. Grosh, and W. B. Cottingham, "Emissivity of weathered conductors after service in rural and industrial environments," *Trans. Am. Inst. Electr. Eng. Part III Power Appar. Syst.*, vol. 81, no. 3, pp. 891–896, 1962.

[10] C. S. Taylor and H. E. House, "Emissivity effects on stranded Aluminum conductors," *Electr. Eng.*, vol. 76, no. 3, p. 195, 1957.

[11] J. Coffey, “High Temperature Overhead Conductor Rating Considerations,” 2018.

[12] A. W. Abboud, J. P. Gentle, K. Parikh, and J. Coffey, “Sensitivity Effects of High Temperature Overhead Conductors to Line Rating Variables,” Idaho National Lab.(INL), Idaho Falls, ID (United States), 2020.

[13] M. Bertinat, R. Wood, and E. Marquand, “Improved Statistical Ratings For Distribution Overhead Lines (Phase 2) Final Report,” 2018.

[14] P. De Bruyne and B. Currat, “Temperature and frequency effects on cable resistance,” *AESA Cortaillod, Switzerland, Tech. Rep. AN1506A*, 2015.

[15] C. Lian, X. Zhang, C. Emersic, and I. Cotton, “Ageing Behaviours of Superhydrophobic and Icephobic Coatings on Overhead Line Systems,” in *2020 IEEE 3rd International Conference on Dielectrics (ICD)*, 2020, pp. 138–141.

[16] G. Momen, M. Farzaneh, and A. Nekahi, “Properties and applications of superhydrophobic coatings in high voltage outdoor insulation: a review,” *IEEE Trans. Dielectr. Electr. Insul.*, vol. 24, no. 6, pp. 3630–3646, 2017.